Comparative Evaluation of AC and DC Power Distribution Systems for Underwater Vehicles Based on Multiobjective Optimization Techniques

Hoai Nam Le, *Member, IEEE,* and Elisabetta Tedeschi, *Senior Member, IEEE*

Abstract—This paper presents a multiobjective optimization technique for the submarine cables of high-power remotely operated vehicles (ROVs). A detailed design flowchart with integrated electrical and mechanical designs of the ROV submarine cables is provided to quantitatively compare AC and DC-based power distribution systems and identify the optimal design from multiple standpoints, prioritizing electrical loss and cable weight. The electromechanical cable design optimization plays a vital role in the ROV industry and in all those applications where the power distribution system is employed vertically from the support platform/vessel. The entire procedure is exemplified by carrying out a particular case study; for an ROV power hub with rated power of 5 MW and operational depth of 6000 m, the DC submarine cable design with distribution voltage of 33 kV results in an electrical loss reduction of 54.3% compared to the AC submarine cable design with distribution voltage of 22 kV at similar cable weights of 63 ton. Additionally, the proposed method can be widely applied to any type of AC-DC comparison to achieve the optimal ROV submarine cable design with a considerably short process time in comparison to the approaches with finite element analysis.

Index Terms—Underwater power cables, medium-voltage power distribution, optimization methods, electromechanical properties, finite element analysis, remotely operated vehicles.

I. Introduction

IN recent years, offshore and subsea activities in deep and ultra-deep water have been continuously developing due to the steep increase in offshore wind farm deployments, oil and gas extraction and other submarine applications such as military, or upcoming deep sea mining. These applications require a high number of so-called "work class" remotely operated vehicles (ROVs), which must satisfy several specifications such as high power demand (from above 200 kW up to several MW), low maintenance, high reliability and capability of operating under extreme conditions [1]–[3]. While the high power demands of manipulators and propulsion so far have been met by hydraulic systems on board, a trend to electrify the high power ROVs has been observed, since reliance on the hydraulic systems for power transmission might reduce their efficiency by 50% [2], [4]. Moreover, recent advances in permanent magnet materials and electro-magnetic motor design

H. N. Le and E. Tedeschi are with the Department of Electric Power Engineering, Norwegian University of Science and Technology, Norway, Hogskoleringen 1, 7491 Trondheim, e-mail: (see https://www.ntnu.edu/employees/hoai.n.le). E. Tedeschi is also with the Department of Industrial Engineering, University of Trento, Trento, Italy.

enable smaller and lighter design for the work class ROVs. Yet, the electrical power distribution design for the ROV applications poses many challenges in the electromechanical design because the whole power distribution system has to be employed vertically from the support platform located at the sea level.

In order to ease the technological transition from the hydraulic system to the fully electric ROVs, the corresponding power distribution grid should be optimized accordingly. Usually, the power required for the ROV operation is generated on the support vessel, and then conveyed to the ROVs located on the sea bottom through AC power cables. Both low voltage (e.g. 440 V or 690 V) and medium voltage (e.g. 3000 V or 6600 V) AC systems, operating at 50 or 60 Hz, are normally used. It is worth noting that, in recent years, the technological transition to all-electric ships has been accelerating significantly to contribute to carbon footprint reduction in marine applications. The solutions usually result in the integration of renewable energy sources and energy storage systems, leading to the employment of DC grids in ships to achieve smart power management [5]–[11]. Therefore, a DC power distribution grid to ROVs might benefit from the further evolutions of these DC ships. Generally, the choice of the voltage level or the distribution frequency poses a trade-off between the electrical and mechanical properties of the power cables (e.g., efficiency the cable weight). Traditional cable design procedures may fail to explore all the possible designs and result in sub-optimal solutions, since the need to meet electrical and mechanical constraints often relies on computationally time-consuming finite element methods (FEM) [4], [12]. Overall, there has been a lack of research on both the efficient, integrated modeling of electromechanical cable properties and their optimization techniques for the ROV applications.

This paper contributes to filling this gap by proposing a multiobjective optimization technique with the combined electrical and mechanical modelling for the ROV submarine cables, which are the backbone of the subsea power distribution system. In particular, the design flowchart is introduced to identify the best configuration from multiple standpoints, while satisfying both the electrical and mechanical specifications. The contributions of this paper to the technological transition towards all-electric ROVs are:

(i) to propose an integrated approach to electromechanical design of submarine cable that is based on mathematical modeling and allows accurate and quick cable modeling, as proved by comparison with traditional FEM [4], [12],

Fig. 1: Power distribution system for high power ROVs.

TABLE I: Main Specifications of ROV Submarine Cables

Rated power	P_r	0.2 - 20 MW
Distribution voltage	V_{AC}	1 kV - 33 kV
	V_{DC}	1 kV - 56 kV
Distribution frequency	f	0 - 50 Hz
Operational depth	h	3000 - 6000 m
Maximum strain	ϵ_{max}	0.5%

(TMS), and the ROV tether. Small ROVs such as micro-ROVs can be fed directly via a neutrally buoyant tether between the support vessel and the vehicle. On the other hand, in the work-class ROV applications, the TMS located on the sea floor is introduced to reduce the effect of drag and vertical movement on the ROVs especially in deep areas. The water current drag force is mitigated by the heavy ROV submarine cables connecting the TMS to the support vessel, and the ROV is fed by a neutrally buoyant tether connected to the TMS. While the ROV tether has almost no weight in water and delivers power to the ROV for few hundred meters, the ROV submarine cable covers the longest power distribution distance up to several thousand meters and has to carry its own weight in water. This configuration poses difficulties in the electrical and mechanical design of the ROV submarine cables. Therefore, the optimization of the power distribution system for the high power ROVs focuses mainly on the ROV submarine cables.

The main objective of this paper is to demonstrate a cable design method, which provides a good selection of design candidates after first screening multiple design alternatives under a specified set of design constraints and standards. More specifically, the electrical and mechanical design of the submarine cable in this paper is conducted based on the International Standards IEC 60502 and 60287, where the highest distribution voltage of the AC submarine cables is 33 kV [14], [15]. With the same insulator wall thickness, the maximum phase-to-neutral DC distribution voltage is designed at the peak value of the phase-to-neutral AC distribution voltage. Consequently, the highest phase-to-phase distribution voltage of the DC submarine cable is higher than that of the AC submarine cable with a factor of approximately $\sqrt{2/3}$, resulting in the 56 kV DC voltage corresponding to the 33 kV voltage in AC distribution. It is worth noting that, the same proposed design procedure can be applied to recent offshore installations where the maximum AC distribution voltage of 66 kV is employed [16]–[18].

Fig. 2 depicts the multiobjective optimization technique for the submarine cable design [19]. The design of a submarine cable involves numerous different design variables such as; the component values (e.g., distribution voltage level, or distribution frequency), materials and geometries. First, the possible combinations of design variable values form the set of possible submarine cable designs, which is referred as the design space. Hence, the design space is visualized as a multidimensional space with each axis representing an individual design variable. Second, the submarine cable characteristics, i.e., electrical and mechanical properties, are derived for each submarine cable design in the design space
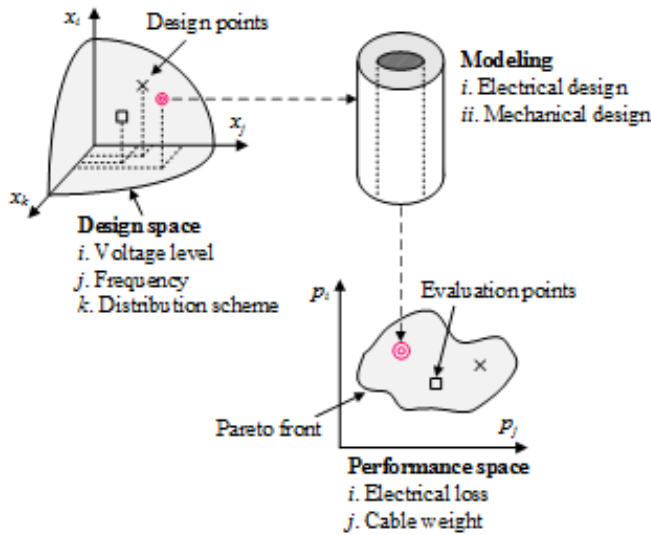
(ii) to develop a multiobjective optimization technique integrating (i) to identify the best configuration,

(iii) the possibility to enable the extension of the proposed approach to a variety of power distribution systems such as, e.g. subsea power supply to oil and gas equipment, or offshore renewable energy applications, by updating the electromechanical constraints and specifications [13].

This paper is organized as follows; section II presents the multiobjective optimization technique for the submarine cables and its systematization through a design flowchart, whereas section III introduces the electrical and mechanical models of the submarine cables. In section IV, the multiobjective optimization of the submarine cables is applied to a test case. The comparison between AC and DC power distribution systems is conducted based on the optimization results.

II. Multiobjective Optimization Technique

This section presents the multiobjective optimization technique proposed for the ROV submarine cables. The first part of this section focuses on the methodology, whereas the last part introduces the design flow chart and software implementation.

A. Methodology

Fig. 1 depicts the typical power distribution system for ROVs, whereas table I shows the main specifications of the ROV submarine cables [1], [3]. The power distribution system for the ROVs considered in this paper consists of three parts: the ROV submarine cables, the tether management system

Fig. 2: Multiobjective optimization technique for ROV submarine cable design.

Fig. 3: Design flowchart representing multiobjective optimization technique.

by the mathematical cable modeling. Finally, the cable performance is calculated from the submarine cable characteristics to obtain the performance space. In this paper, the submarine cable performance is defined by the pair of the electrical loss P_{loss}, and the submarine cable weight in air m_c. Usually, the performance space results in the Pareto front, i.e., the set of designs that offer the best possible tradeoffs among P_{loss}, and m_c. The Pareto front in the performance space can be used to identify the combination of design variable values in the design space that achieves the highest performance while complying with the specifications and constraints.

B. Flowchart

Fig. 3 depicts the design flowchart representing the multiobjective optimization technique, i.e., the mapping of the design points in the design space, into the evaluation points in the performance space to form the Pareto front. In particular, the required inputs are the design variables, constraints, system specifications, and the material database. The output is the set of Pareto-optimal submarine cable designs.

1) Search Algorithm: The proposed optimization flowchart classifies the design variables into the following two categories:

(i) Electrical design variables $\vec{x}_{ele}$, which are the submarine voltage level V_{dis}, and the distribution frequency f_{dis}.

(ii) Mechanical design variables $\vec{y}_{mec}$, which are the armor design variables (wire diameters d_A, and wire helix angles α_A).

This distinction of the design variables results in the electrical and mechanical design loops as shown in Fig. 3. The electrical design variables $\vec{x}_{ele}$ are iterated in an outer loop, where for each iteration i, a new set of the under-armor submarine cable configuration is obtained. Then, based on each under-armor submarine cable configuration, the armor is optimized in the inner loop that iterates the corresponding mechanical
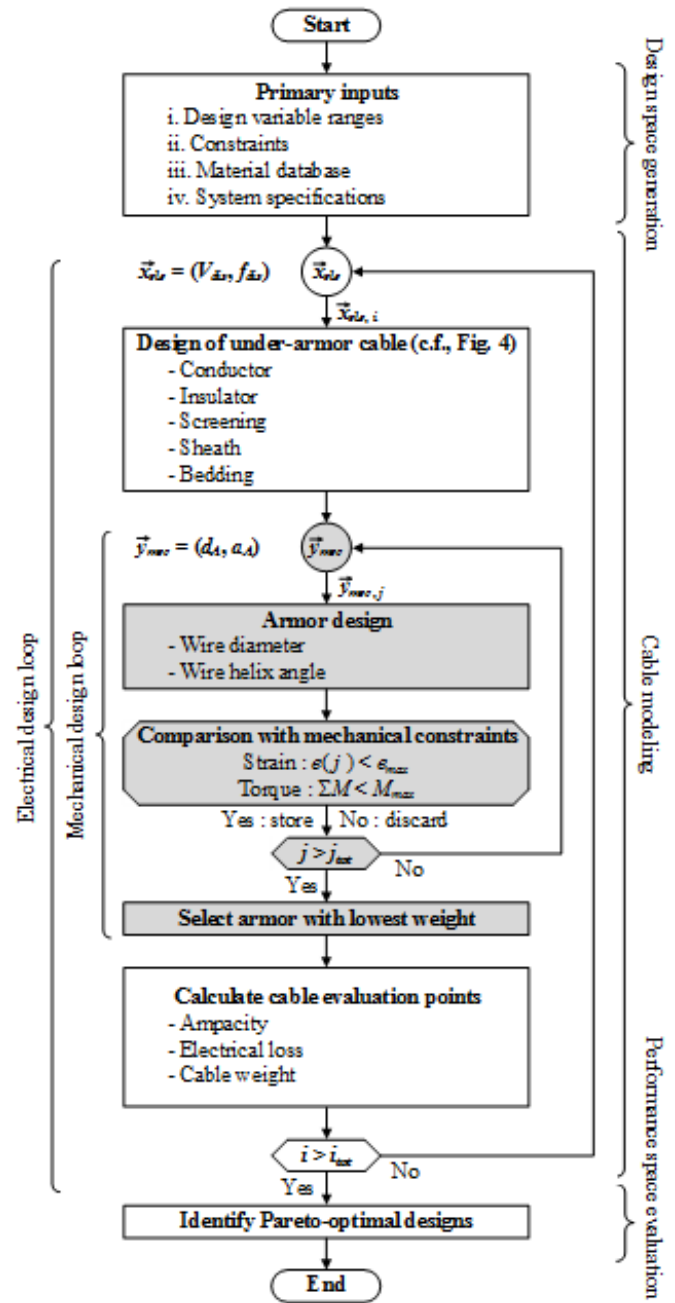
design variables $\vec{y}_{mec}$. The goal of the mechanical design loop is to identify the armor design variable value $\vec{y}_{mec}$ which achieves the lowest weight in air while complying with mechanical constraints (e.g., the maximum strain at working load, and the torque balance). The advantage of this design variable classification is the reduction of the optimization complexity: only the armors of the under-armor submarine cable configurations that comply with the electrical constraints are considered in the mechanical design loop. In the next step, the properties of the submarine cable evaluation points (e.g., the ampacity, the electrical loss, the cable weight, and the material cost) within the iteration i of the outer loop

are calculated to form a corresponding evaluation point in the performance space. Finally, after the iteration of all i_{tot} submarine cable design variable options $\vec{x}_{ele}$, the Pareto front is identified as the boundary of the evaluation points in the performance space.

2) Software Implementation: The proposed design flowchart is implemented in MATLAB. The code encompasses approximately 1012 lines, of which 25% is dedicated to the armor design. MATLAB is chosen mainly because it can provide a large options for handling complex data structures and numerical methods. However, any similar software can also be utilized because the code for the design flowchart is constructed basically from the loop control statements, the conditional statements and the numerical equations.

III. CABLE MODELING

This section presents a brief overview of the electrical and mechanical models used in the design flowchart of Fig. 3. The first part of this session introduces the electrical and mechanical models of the the submarine cable, whereas the last part confirms the validation of these models by providing the calculation results with FEM.

A. Electrical Design

Fig. 4 depicts the ROV medium voltage submarine cables with separate screened cable configuration [20], [21]. The two-core cable transmits the DC current, whereas the three-core cable represents the AC cable. First, the dimensions of the under-armor cable are determined to comply with the international standards IEC-60502 and IEC-60287 [14], [15]. In other words, the electrical design of the ROV submarine cable, i.e. the under-armor cable design, is conducted similarly to general underwater power cables. Then, the electrical properties, i.e. the current rating, the loss factors, and the thermal and electrical resistances, are derived.

1) Cable Material Selection:

a) Conductor: The conductor of the submarine cables can be made of copper or aluminum. Copper conductors are more resistant against corrosion, and also have a higher fatigue resistance and breaking strength than aluminum conductors. Consequently, only copper conductors are considered in this paper. First, the conductor cross-sectional area is selected in the range of 10 mm^2 and 1600 mm^2. Then, the wall thicknesses of the insulation, screening, sheath and bedding are selected accordingly to IEC-60502 [15].

b) Insulation: The insulation of the medium voltage submarine cable can be provided by cross-linked polyethylene (XLPE) or ethylene propylenen rubber (EPR) [22]. Compared to oil filled paper insulated submarine cables, XLPE and EPR offer following advantages: free maintenance, lighter weight, and lower sensitivity to severe stresses to which the submarine cables are subject during transportation, laying and operation.

c) Screen, sheath, fillers and bedding: The conductor and insulation screens are the semi-conductive layers whose main purpose is to obtain a uniform distribution of the electric field within the insulation. As the conductor is stranded, its surface is only approximately cylindrical. In the absence of the
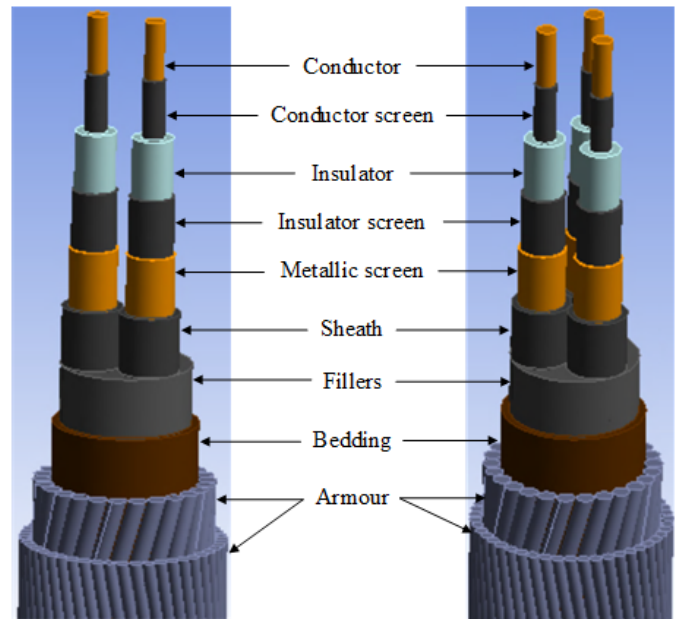

Fig. 4: ROV medium voltage submarine cables with SL configuration.

conductor semi-conductive layers, the electric field might become concentrated at certain points, leading to local dielectric breakdown. The insulation semi-conductive layers are applied for the same reason. Meanwhile, the metallic screens confine the electric field of the cable within the insulation surrounding the conductor by safely carrying the cable charging current to a solid ground point. Consequently, the metallic screens, which can be made from helically applied and overlapped copper tapes, are generally connected to the ground points at both ends of the medium voltage submarine cable. The sheath protects the underlying cable core from mechanical, moisture and chemical damage during the installation and service life of the cable. The material choice for the sheath is normally polyethylene (PE). The fillers and bedding are made of PE strings to fill the spaces between the cores and make the cable round while providing a protective boundary between inner and outer layers of the cable.

2) Derivation of Electrical Properties:

a) Current rating: The current rating I_{AC}, I_{DC} for the AC and DC submarine cables are defined by [14],

$$I_{AC} = \left[\frac{T_c - T_{amb}}{R_{AC}R_{th1} + nR_{AC}(1+\lambda_1)R_{th2} \\ + nR_{AC}(1+\lambda_1+\lambda_2)R_{th3}} \right]^{0.5} \quad (1)$$

$$I_{DC} = \left[\frac{T_c - T_{amb}}{R_{DC}R_{th1} + nR_{DC}R_{th2} + nR_{DC}R_{th3}} \right]^{0.5} \quad (2)$$

where T_c is the maximum operating temperature, T_{amb} is the ambient temperature, R_{AC}, R_{DC} are the AC and DC resistances per unit length of the cable at T_c, n is the number of load-carrying conductors in the cables, λ_1 is the ratio of losses in the metal screens to total losses, λ_2 is the ratio of losses in the armours to total losses, R_{th1}, R_{th2}, and R_{th3} are

the thermal resistances per unit length between one conductor and the sheath, between the sheath and the armour, between the armour and the surrounding medium, respectively.

b) Electrical resistances and loss factors: The electrical loss in the submarines cables consists of losses in the insulators, the conductors, the metallic screens, and the armours. The dielectric loss in the insulators is mainly due to friction losses from dipoles rotating with the voltage frequency. For medium voltage cables, because the capacitance is much smaller compared to that in high voltage applications, the dielectric loss in the insulators can be considered negligible [23]. Meanwhile, the losses in the metallic screens and the armours are normalized to the loss in the conductors by loss factors λ_1 and λ_2 according to IEC-60287. Therefore, first the AC resistance of the conductors R_{AC} is calculated as,

$$R_{AC} = R_{DC}(1 + y_s + y_p) \tag{3}$$

where y_s and y_p are the skin effect and proximity effect factors, respectively. Then, y_s and y_p are defined in,

$$y_s = \begin{cases} \dfrac{x_s^4}{192 + 0.8x_s^4}, & \text{if } x \leq 2.8 \\ 0.136 - 0.0177x_s + 0.0563x_s^2, & \text{if } 2.8 < x \leq 3.8 \\ 0.354x_s - 0.733, & \text{if } x > 3.8 \end{cases} \tag{4}$$

$$y_p = \dfrac{x_p^4}{192 + 0.8x_p^4}\left(\dfrac{d_c}{s}\right)^2$$

$$* \left[0.312\left(\dfrac{d_c}{s}\right)^2 + \dfrac{1.18}{\dfrac{x_p^4}{192 + 0.8x_p^4} + 0.27}\right] \tag{5}$$

$$x_s = x_p = \sqrt{\dfrac{8\pi f}{R_{DC}}10^{-7}} \tag{6}$$

where d_c is the conductor diameter, s is the distance between conductor axes, and f is the distribution frequency. The electrical loss in the metallic screens is caused by circulating currents and eddy currents. As the metallic screens in the submarine cables are bonded at both ends, only the loss due to circulating currents needs to be considered [24]. Then, λ_1 is defined in,

$$\lambda_1 = \lambda_1' = \dfrac{R_s}{R_{AC}}\dfrac{1.5}{1 + \left(\dfrac{R_s}{X}\right)^2} \tag{7}$$

$$X = 4\pi f 10^{-7}\left(\dfrac{2s}{d}\right) \tag{8}$$

where R_s is the DC resistance of the metallic screens at the maximum operating temperature, and d is the mean diameter of the metallic screens. Finally, λ_2 is approximated in,

$$\lambda_2 = \dfrac{2.48(\pi f)^2 10^{-14}}{R_{AC}R_A} + \dfrac{7.64A\pi f 10^{-5}(1.48r_1 + t)^2}{R_{AC}(d_A^2 + 95.7A)^2} \tag{9}$$

where R_A is the AC resistance of the armour at maximum operating temperature, d_A is the mean diameter of armour, A is the cross-sectional area of armour, r_1 is the circumscribing radius over conductors, and t is the insulation thickness between conductors. It should be noted that several publications have been reported to improve the metallic screen and armour loss calculation error compared to the methods employing IEC-60827 [24]–[26]. Therefore, the improved metallic screen and armour loss calculation can be substituted into (7)-(9) to further improve the accuracy of the total loss calculation of the submarine cables.

c) Thermal resistances: The thermal resistances are derived dependently on the configuration of the submarine cables (cf. Fig. 4). The thermal resistances between one conductor and the sheath of 2-core cable and 3-core cable R_{th1_2}, R_{th1_3} are defined in,

$$R_{th1_2} = \dfrac{\rho_T}{2\pi}ln\left(1 + \dfrac{2t_1}{d_c}\right) \tag{10}$$

$$R_{th1_3} = \dfrac{\rho_T}{2\pi}G \tag{11}$$

where ρ_T is the thermal resistivity of insulator, t_1 is the thickness of insulation between conductor and sheath, and G is the geometric factor given in Fig. 3 of [14]. Then, the thermal resistance between the sheath and the armour R_{th2} is defined in,

$$R_{th2} = \dfrac{\rho_f}{6\pi}\overline{G} \tag{12}$$

where ρ_f is the equivalent thermal resistance of the sheath, the fillers and the bedding, and $\overline{G}$ is the geometric factor given in Fig. 6 of [14]. Next, the thermal resistance between the armour and the surrounding medium R_{th3} is approximated as,

$$R_{th3} = \dfrac{\rho_{amb}}{2\pi}ln\left(\dfrac{2h}{D_e}\right) \tag{13}$$

where ρ_{amb} is the thermal resistance of the surrounding medium, h is the operation depth, and D_e is the external diameter of the cable. Note that the armour parameters are obtained in section III.B.

B. Mechanical Design

The submarine cable for ROV normally experiences high tension and strain during its installation and recovery due to its long suspended length in deep ocean [27]. Armour stranded wires are employed in the submarine cable design to keep the cable strain below a prescribed level. Moreover, the submarine cable might develop torque when subjected to tension, further worsening the cable strain. Consequently, the multi-layer configuration of the armour is generally applied to the cable design [28]. By wrapping the armour layers in opposite directions, the balance net torque can be produced. The mechanical design goal of the submarine cables is to identify the armour parameters, i.e. the wire diameter d_A and helix angle α, satisfying the maximum strain level and the
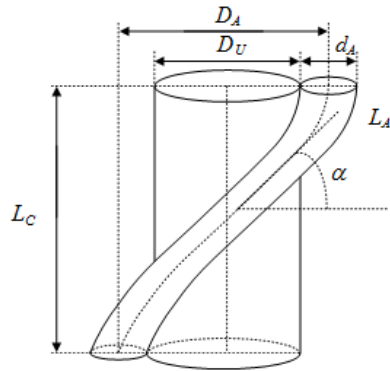
Fig. 5: Analysis model of submarine cable with single armour layer.

Fig. 6: ROV submarine cable and TMS in suspension during recovery.

torque balance. For the sake of simplicity, only two-armour-layer configuration is considered, but the same reasoning can in principle be applied to a higher number of layers.

The derivation of the armour parameters is provided as follows; first, each combination of the wire diameters and the helix angles for each armour layer is generated. For each individual combination, the tension, strain and torque of the cable are calculated and compared with the mechanical constraints, i.e. the maximum strain level and the balance torque. The armour parameter combinations that comply with the mechanical constraints, are then compared to each other in term of the armour weight to find the smallest armour weight. In other words, the mechanical design loop goal is to find the armour parameters that result in the smallest armour weight while satisfying the mechanical constraints.

1) Tensile and Torsional Properties: Fig. 5 depicts the analysis model of the submarine cable with single armour layer [28]. The relations among the total axial load T_t, the total cable moment M_t and the cable strain ϵ_c with the cable ends twist-restrained are defined by,

$$\epsilon_c = \frac{T_t}{C_3} \tag{14}$$

$$M_t = C_1 \epsilon_c \tag{15}$$

where C_1 and C_3 are the coefficients calculated by,

$$C_1 = \sum_{k=1}^{2} (\sin^2 \alpha_k - \gamma_k^* \cos^2 \alpha_k)^2 E_{Ak} n_{Ak} A_{Ak} r_{Ak} \cos \alpha_k \tag{16}$$

$$C_3 = E_c A_c + E_{ms} A_{ms} + \sum_{k=1}^{2} (\sin^2 \alpha_k - \gamma_k^* \cos^2 \alpha_k)^2 E_{Ak} n_{Ak} A_{Ak} \sin \alpha_k \tag{17}$$

where γ_k^* is the pseudo-Poisson's ratio for the kth armour layer and is the measure of the armour diametric contraction, E_{Ak} is the tensile modulus of the armour wires, n_{Ak} is the armour wire number, A_{Ak} is the cross-sectional area of a single armour wire, and r_{Ak} is the pitch radius of the armour; whereas the subscripts c and ms refer to the conductor and the metallic screen, respectively. Since n_{Ak}, A_{Ak} and α_k
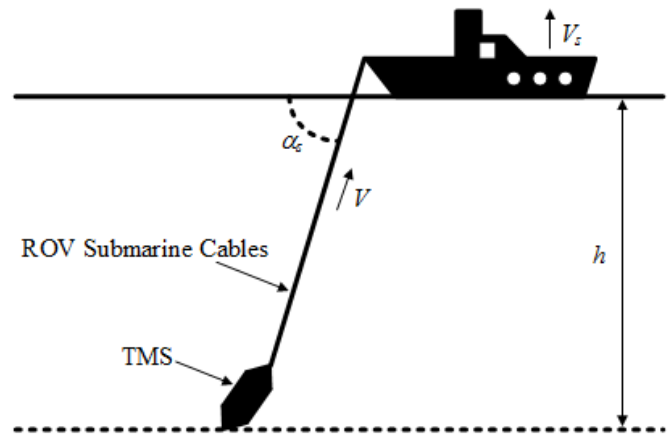
change accordingly to d_A and α, then C_1 and C_3 are also recalculated for each combination of d_A and α. In particular, n_A is calculated by,

$$n_A = \frac{\pi}{\sin^{-1}\left(\frac{d_A}{D_U + d_A}\right)} * K_A \tag{18}$$

where D_U is the fictitious diameter under armour, and K_A is the fill factor of the armour. Then, T_t is derived in the following subsection to calculate ϵ_c.

2) Cable Tension during Recovery: Fig. 6 depicts the ROV submarine cable and the TMS in suspension during recovery [27]. Cable tension at the overboard sheave in the support vessel is higher than in any other handling operations. Therefore, the mechanical design is conducted considering the recovery operation condition. There are three components contributing to T_t: the quasi-static tension induced by the recovery speed T_1, the dynamic cable tension caused by the ship motion T_2, and the additional tension caused by the TMS weight T_3. First, T_1 is calculated by using Zajac's method,

$$T_1 = \frac{wh}{1 - \left[\tan^2\left(\frac{\alpha_c}{2}\right)\left(\frac{\cos \alpha_c + \cos \alpha_s}{1 - \cos^2 \alpha_c}\right)\right]^{1/\gamma}} \tag{19}$$

where w is the cable weight per unit length in water, h is the operational depth, α_s is the outboard angle between the cable and the sea, α_c and γ are the critical and ascent angles which are defined by,

$$\alpha_c = \cos^{-1}\left[\sqrt{1 + \frac{1}{4}\left(\frac{H}{V}\right)^4 - \frac{1}{2}\left(\frac{H}{V}\right)^2}\right] \tag{20}$$

$$\gamma = \frac{2 - \sin^2 \alpha_c}{\sin^2 \alpha_c} \tag{21}$$

where V is the recovery speed, and H is the cable hyrodynamic constant which is expressed by,

TABLE II: Mechanical and electrical data of submarine cables

Cable parameters (cf., Fig.4)	Three cores	Two cores
Voltage level [kV]	18 / 30 (36)	0.6 / 1.0 (1.2)
Nominal area of conduction [mm^2]	120	50
Conductor screen wall thickness [mm]	0.46	0
Insulation XLPE wall thickness [mm]	8.0	1.0
Insulation screen wall thickness [mm]	0.5	0
Metallic screen cross sec. area [mm^2]	16	0
Sheath wall thickness [mm]	2.5	0
Bedding wall thickness [mm]	2.0	2.0
Wire diameter of armour layer 1 [mm]	4.05	1.6
Wire diameter of armour layer 2 [mm]	3.15	1.6
Helix angle of armour layer 1 [mm]	73.3	73.3
Helix angle of armour layer 2 [mm]	69.0	78.4
Cable weight in air [kg/m]	20.3	3.1
Current rating [A]	308.5	191.8
Electrical losses [W/m]	60.8	36.3

$$H = \sqrt{\frac{2w}{C_D \rho D_e}} \qquad (22)$$

where C_D is the drag coefficient that translates the friction exerted by the seawater mass on the cable in the direction perpendicular to it, ρ is the seawater density, and D_e is the external diameter of the cable.

Next, the dynamic cable tension caused by the ship motion T_2 is calculated by,

$$T_2 = \sqrt{C_3 m_C} V_s \qquad (23)$$

where V_s is the support vessel's vertical velocity, and m_C is the cable mass per unit length.

Finally, the additional tension induced by the TMS weight T_3 is expressed as,

$$T_3 = w_T + m_T a_s \qquad (24)$$

where w_T is the TMS weight in water, m_T is the TMS mass, and a_s is the vertical acceleration of the support vessel. For the sake of simplicity, T_3 is considered to be negligibly small in this paper assuming that the TMS's thrusters support it during the recovery. Substitution of the above expressions for T_t into (1) and (2) gives the tensile and torsional properties of the cable under twist-restraint condition.

C. Finite Element Analysis

Table II depicts the mechanical and electrical data of two submarine cables which are designed based on the flow chart in Fig. 3 and Table I. ANSYS is employed as the finite element software, where FEM is applied to simulate the tension tests of the submarine cables [4], [12]. First, the geometric models of the submarine cable are constructed in ANSYS/Geometry (Toolbox of Static Structural). Then, these geometric models are imported to ANSYS/Model to obtain the strain under the tension test. Note that only the geometrically linear behaviour of the cables is considered because the submarine cables are assumed to work within the elastic region.

Fig. 7 depicts the elongation of the three-core submarine cable model under tension test. The initial length of the three-core cable is 100 mm. Under the tension force of 1273.2 kN which is assumed as the maximum load applied to the
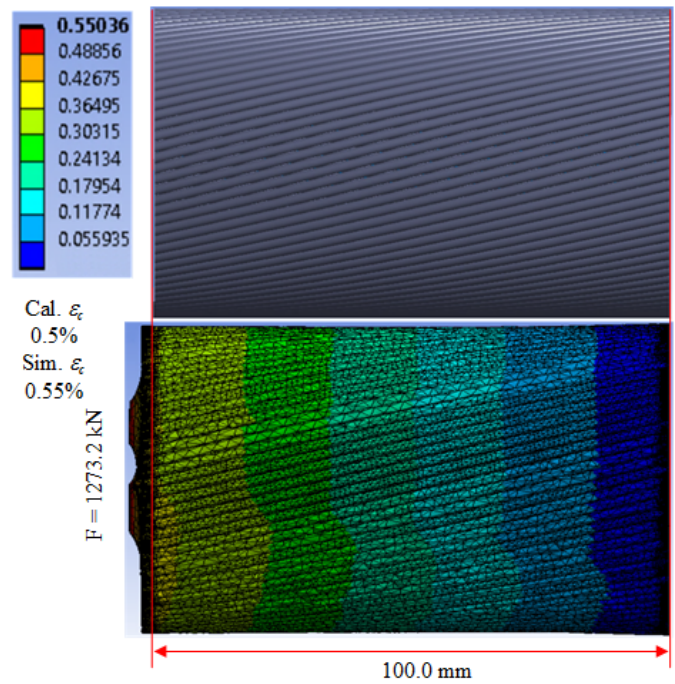

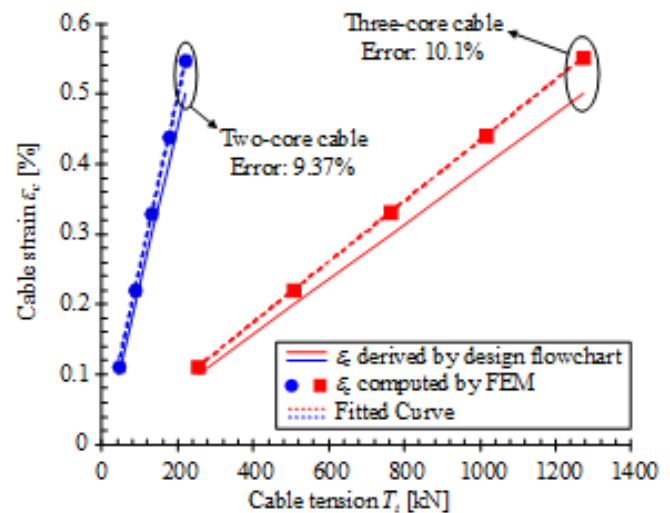Fig. 7: Elongation of three-core submarine cable model under tension test.

Fig. 8: Comparison of cable strain versus cable tension computed according to design flowchart and FEM.

cable during the recovery (cf., (6)-(10) in section III.B), the resultant elongation of the three-core cable model is 0.55 mm. Therefore, the calculated strain with FEM is 0.55%, resulting in the error of approximately 10% when comparing with the theoretical strain of 0.5%.

Fig. 8 depicts the comparison of the cable strain versus the cable tension computed either by means of the design flowchart or FEM. The tension forces applied to the two-core cable are 44.2 kN, 88.3 kN, 132.5 kN, 176.7 kN and 220.1 kN, whereas the tension forces applied to the three-core cable are 254.6 kN, 509.3 kN, 763.9 kN, 1018.6 kN and

TABLE III: Optimization coefficients and constraints

Rated power [MW]	P_r	5
Operational depth [m]	h	6000
Nominal ambient temperature [°C]	T_{amb}	20
Max. conductor temperature [°C]	T_c	90
Tensil modulus of copper [GPa]	E_{copper}	110
Tensil modulus of steel [GPa]	E_{steel}	200
Pseudo-Poisson's ratio	γ_k^*	0.3
Outboard angle [degree]	α_s	75
Cable recovery speed [m/s]	V	0.5
Seawater drag coefficient	C_D	1.5
Seawater density [kg/m^3]	ρ	1050
Support vessel's vertical velocity [m/s]	V_s	3

1273.2 kN. Such tension forces are selected at 20%, 40%, 60%, 80% and 100% of the maximum load applied to the cable during the recovery respectively. Smaller tension forces are applied to the two-core cable compared to those of the three-core cable, because the two-core cable weight in air is lower than the weight of the three-core cable. The errors between the derived-by-design-flowchart and FEM strains of the two-core and three-core cable models are 9.37% and 10.1%, respectively. Note that same errors are obtained in 5 points of the applied tension force in both the cases of the two-core and three-core cable models. In practice, the submarine cables are usually designed with the safety factor higher than 2 [1], [27]; therefore, the errors between the derived-by-design-flowchart and FEM strains are considered to be small, validating the mechanical design in section III.B.

IV. PERFORMANCE SPACE ANALYSIS

This section presents the optimization results using a specific case study as an example.

Table III lists the optimization coefficients and constraints. In this section, the multiobjective optimization technique (cf., Fig. 3) is employed to find the Pareto fronts of the AC and DC submarine cable designs with the optimization parameters listed in Table I and Table III. The entire procedure is exemplified by carrying out a particular case study for an ROV power hub with rated power of 5 MW and operational depth of 6000 m. For recovery in adverse conditions, the following assumptions are made; the outboard angle at the support vessel α_s is 75°C, and the maximum support vessel's vertical velocity V_s is 3 m/s. The two-core cable configuration is employed as the DC submarine cable, whereas the three-core cable is used as the AC submarine cable (cf., Fig. 4). Instead of the employment of FEM for all the design points in the design space (cf., Fig. 2), the mechanical design introduced in section III.B significantly reduces the process time of the multiobjective optimization technique. For instance, the process time of FEM for only one design point is approximately 12 hours, including the model construction, the mesh generation and the solution calculation. Note that the parallel processing of ANSYS is employed to the mesh generation and the solution calculation with the aim to reduce the process time. Specifically, the whole process of FEM is implemented to a server computer with 28 cores, whose base speed of each core is 2.6 GHz. On the other hand, the multiobjective optimization technique based on the proposed mechanical design is employed to a laptop

(a) m_c-P_{loss} Pareto front of AC submarine cable designs

(b) m_c-P_{loss} Pareto front of DC submarine cable designs

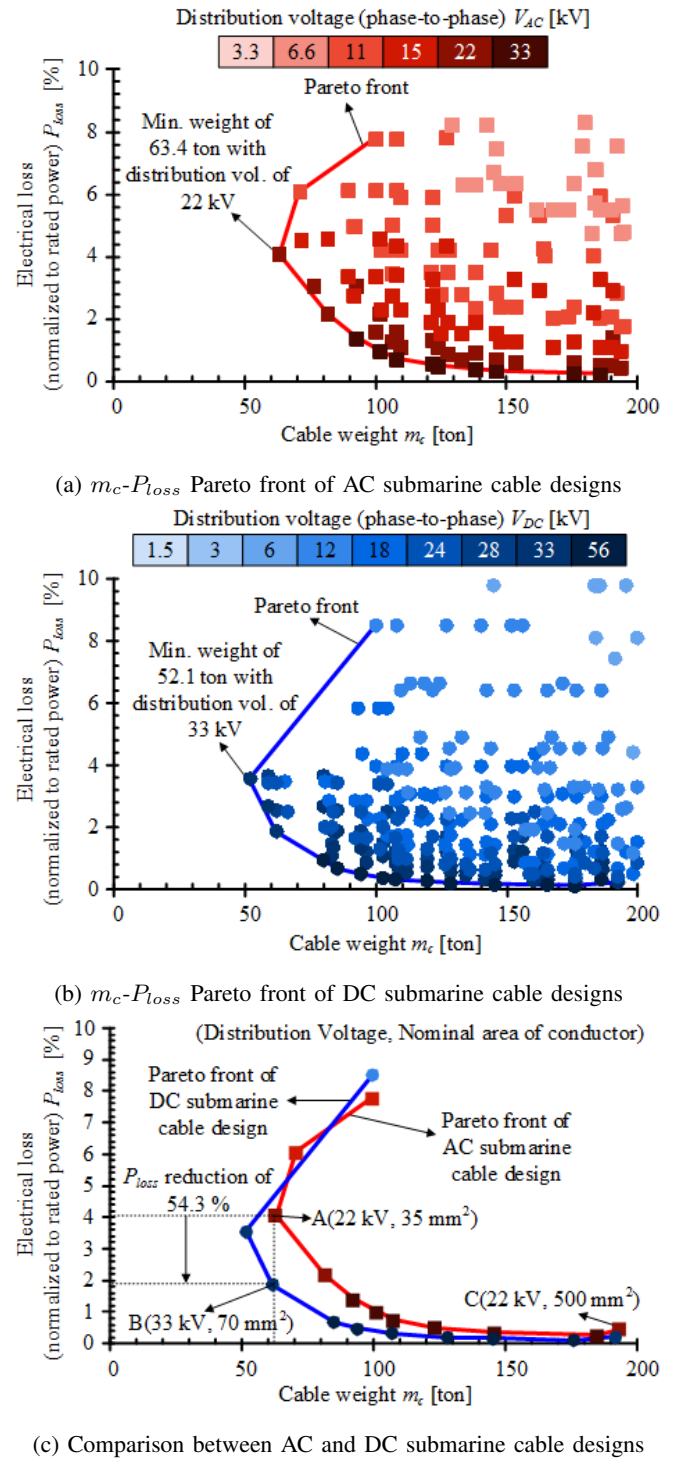(c) Comparison between AC and DC submarine cable designs

Fig. 9: Performance space of AC and DC submarine cables in term of electrical loss and cable weight.

with 2 cores, whose base speed of each core is 1.9 GHz, and takes approximately 3 hours to evaluate *all* possible design points, enabling the designer to achieve the optimal design in a considerably short time and low-cost hardware.

Fig. 9 depicts the performance space of AC and DC submarine cables in term of the electrical loss P_{loss} and the cable weight m_c. As the horizontal and vertical axes present m_c
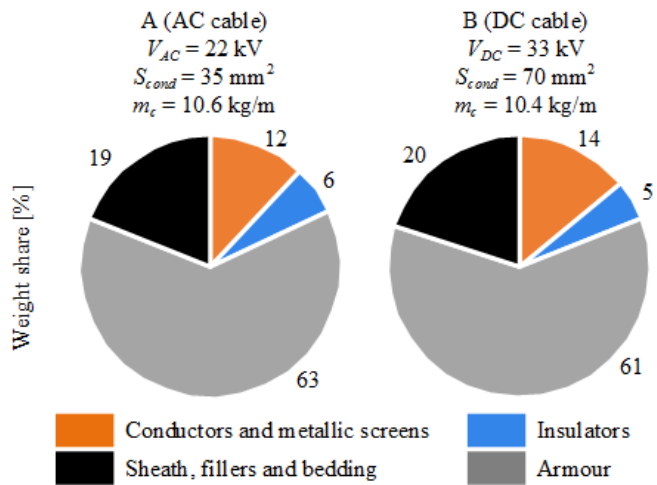
(a) Weight share of selected AC and DC submarine cable designs
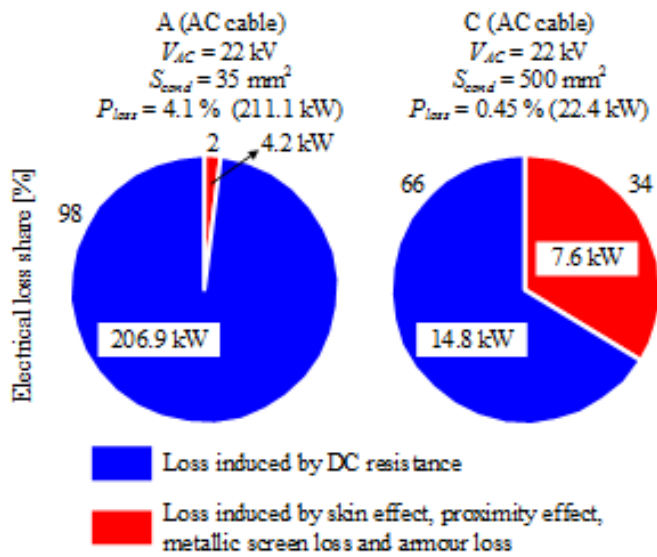
(b) Electrical loss share of selected AC submarine cable designs

Fig. 10: Weight and loss analysis of selected AC and DC submarine cable designs.

and P_{loss} respectively, the evaluation points which are close to the origin feature better submarine cable designs. Hence, the Pareto front of the submarine cable designs is the boundary of the evaluation points which is close to the origin. As observed in Fig. 9a and Fig. 9b, the increase in the distribution voltage reduces the electrical loss due to the decrease in the cable current. Nevertheless, the high distribution voltage does not always result in the minimum cable weight. In particular, the minimum weights of the AC and DC submarine cable designs are 63.4 ton and 52.1 ton with the distribution voltage of 22 kV and 33 kV, respectively. As shown in Fig. 9c, the DC submarine cable designs provide better P_{loss}-m_c trade-off relation compared to that of the AC submarine cable designs. For instance, the design point B with the DC distribution voltage of 33 kV and the nominal conductor area of 70 mm^2 results in the P_{loss} reduction of 54.3% compared to the design point A with the AC distribution voltage of 22 kV and the

nominal conductor area of 35 mm^2 at almost equal m_c of approximately 63 ton.

Fig. 10 depicts the weight and loss analysis of the selected AC and DC submarine cable designs. It is observed from Fig. 10a that the armour occupies the majority of the cable weight. The amount of copper and insulator in the DC cable is almost the same as that in the AC cable, whereas the electrical loss of the DC cable is reduced by 54.3% compared to that of the AC cable (cf., Fig. 9c). As shown in Fig. 10b, the AC loss, i.e. the loss induced by the skin effect, and proximity effect, the metallic screen loss and the armour loss, occupies only a small percentage of the total electrical loss of the AC cables with small conductor nominal cross-sectional area. Meanwhile, the AC cables with large conductor area suffer larger AC loss, e.g. the AC loss results in 34% of the total electrical loss of the AC cable with the conductor cross-sectional area of 500 mm^2. Even though the total loss decreases in the AC cables with large conductor area, the AC loss in the AC cable with the conductor cross-sectional area of 500 mm^2 increases to 7.6 kW compared to the AC loss of 4.2 kW in the AC cable with the conductor cross-sectional area of 35 mm^2. The electrical loss reduction over 50% by the employment of the same-weight DC submarine cable compared to the AC counterpart can substantially contribute to the total cost reduction of the ROV applications, where the main energy source of the support vessel has to be transported from onshore [29]. Furthermore, the DC power distribution system can also eliminate AC-DC conversion step for the motor system, resulting in more compact, light weight and low cost designs for the ROVs.

V. CONCLUSION

In order to support the identification of more efficient powering solutions for the ROV sector, which is transitioning towards more- or fully-electrical solutions, this paper proposed the multiobjective optimization algorithm to assess the best ROV cable configuration, considering both mechanical and electrical aspects. Its application to the selected test case of a 5MW ROV power hub, highlighted that, scarcely investigated DC cable solutions could provide a loss reduction higher than 53% compared to a standard AC cable solution of comparable weight or could otherwise result in a 18% weight reduction for a corresponding power delivery. Comparison with traditional FEM simulations proved that the proposed tool provides an accuracy in the range of 10% being significantly less computationally demanding. Furthermore, the proposed methodology could also be adapted to the assessment of AC and DC solutions for other cable applications such as subsea power supplies for oil and gas extraction or power distribution grids in offshore renewable energy applications.

REFERENCES

[1] H. Nakajoh, H. Osawa, T. Miyazaki, K. Hirata, T. Sawa, and H. Utsugi, "Development of work class rov applied for submarine resource exploration in jamstec," in *2012 Oceans - Yeosu*, 2012, pp. 1–5.

[2] Feng Zhou, Linyi Gu, Gaosheng Luo, Jiawang Chen, Mengjun Zheng, Zongze Shao, and Chunming Dong, "Development of a hydraulic propulsion system controlled by proportional pressure valves for the 4500m work-class rov," in *2013 OCEANS - San Diego*, 2013, pp. 1–6.

[3] G. Spagnoli, S. A. Miedema, C. Herrmann, J. Rongau, L. Weixler, and J. Denegre, "Preliminary design of a trench cutter system for deep-sea mining applications under hyperbaric conditions," *IEEE Journal of Oceanic Engineering*, vol. 41, no. 4, pp. 930–943, 2016.

[4] B. Gustavsen, A. Bruaset, J. J. Bremnes, and A. Hassel, "A finite-element approach for calculating electrical parameters of umbilical cables," *IEEE Transactions on Power Delivery*, vol. 24, no. 4, pp. 2375–2384, 2009.

[5] "Ring network for multi-megawatt dc power system," October 2013. [Online]. Available: http://theswitch.com/wp-content/uploads/2013/10/Marine_Brochure_EN_DC-HUB_Web_20171122.pdf

[6] J. O. Lindtjørn, "Onboard dc grid – a system platform at the heart of shipping 4.0," October 2017. [Online]. Available: https://new.abb.com/marine/generations/generations-2017/business-articles/onboard-dc-grid-a-system-platform-at-the-heart-of-shipping.

[7] G. Sulligoi, A. Tessarolo, V. Benucci, A. Millerani Trapani, M. Baret, and F. Luise, "Shipboard power generation: Design and development of a medium-voltage dc generation system," *IEEE Industry Applications Magazine*, vol. 19, no. 4, pp. 47–55, 2013.

[8] F. D. Kanellos, G. J. Tsekouras, and J. Prousalidis, "Onboard dc grid employing smart grid technology: challenges, state of the art and future prospects," *IET Electrical Systems in Transportation*, vol. 5, no. 1, pp. 1–11, 2015.

[9] Z. Jin, G. Sulligoi, R. Cuzner, L. Meng, J. C. Vasquez, and J. M. Guerrero, "Next-generation shipboard dc power system: Introduction smart grid and dc microgrid technologies into maritime electrical networks," *IEEE Electrification Magazine*, vol. 4, no. 2, pp. 45–57, 2016.

[10] M. Belkhayat, "Ship electrification: Dc versus ac and the rise of digital power [technology leaders]," *IEEE Electrification Magazine*, vol. 5, no. 3, pp. 88–86, 2017.

[11] Z. Jin, L. Meng, J. M. Guerrero, and R. Han, "Hierarchical control design for a shipboard power system with dc distribution and energy storage aboard future more-electric ships," *IEEE Transactions on Industrial Informatics*, vol. 14, no. 2, pp. 703–714, 2018.

[12] Y. Hu, Z. Hu, H. Ma, P. Yan, and Y. Liu, "Finite element simulation of axial elastic characteristics of wire rope with one round strand layer," in *2016 IEEE 20th International Conference on Computer Supported Cooperative Work in Design (CSCWD)*, 2016, pp. 16–19.

[13] J. Robinson, D. Jovcic, and G. Joos, "Analysis and design of an offshore wind farm using a mv dc grid," *IEEE Transactions on Power Delivery*, vol. 25, no. 4, pp. 2164–2173, 2010.

[14] *Electric cables – Calculation of the current rating –*, International Standard IEC 60287, 1993-2015.

[15] *Power cables with extruded insulation and their accessories for rated voltage from 1 kV (U_m = 1.2 kV) up to 30 kV (U_m = 1.2 kV)*, International Standard IEC 60502, 2009-2014.

[16] H. Ahmad, S. Coppens, and B. Uzunoglu, "Connection of an offshore wind park to hvdc converter platform without using offshore ac collector platforms," in *2013 IEEE Green Technologies Conference (GreenTech)*, 2013, pp. 400–406.

[17] S. Gasnier, V. Debusschere, S. Poullain, and B. François, "Technical and economic assessment tool for offshore wind generation connection scheme: Application to comparing 33 kv and 66 kv ac collector grids authors," in *2016 18th European Conference on Power Electronics and Applications (EPE'16 ECCE Europe)*, 2016, pp. 1–8.

[18] L. F. N. Lourenco, N. Suzuki, R. M. Monaro, and M. B. C. Salles, "Economical evaluation of an isolated ac offshore grid for pre-salt oil production based on power hub for reducing carbon emissions," in *2019 8th International Conference on Renewable Energy Research and Applications (ICRERA)*, 2019, pp. 450–454.

[19] R. M. Burkart and J. W. Kolar, "Comparative life cycle cost analysis of si and sic pv converter systems based on advanced η- ρ-σ multiobjective optimization techniques," *IEEE Transactions on Power Electronics*, vol. 32, no. 6, pp. 4344–4358, 2017.

[20] H. Tayama, O. Fukuda, K. Yamamoto, Y. Inoue, and Y. Koike, "6.6 kv xlpe submarine cable with optical fiber sensors to detect anchor damage and defacement of wire armor," *IEEE Transactions on Power Delivery*, vol. 10, no. 4, pp. 1718–1723, 1995.

[21] R. Benato, S. Dambone Sessa, and M. Forzan, "Experimental validation of three-dimension multiconductor cell analysis by a 30 km submarine three-core armoured cable," *IEEE Transactions on Power Delivery*, vol. 33, no. 6, pp. 2910–2919, 2018.

[22] Y. Liu, X. Cao, and M. Fu, "The upgrading renovation of an existing xlpe cable circuit by conversion of ac line to dc operation," *IEEE Transactions on Power Delivery*, vol. 32, no. 3, pp. 1321–1328, 2017.

[23] A. Burstein, V. Cuk, and E. D. Jong, "Determining potential capacity gains when repurposing mvac cables for dc power transportation," *CIRED - Open Access Proceedings Journal*, vol. 2017, no. 1, pp. 1691–1694, 2017.

[24] J. S. Barrett and G. J. Anders, "Circulating current and hysteresis losses in screens, sheaths and armour of electric power cables-mathematical models and comparison with iec standard 287," *IEE Proceedings - Science, Measurement and Technology*, vol. 144, no. 3, pp. 101–110, 1997.

[25] K. F. Goddard, J. A. Pilgrim, R. Chippendale, and P. L. Lewin, "Induced losses in three-core sl-type high-voltage cables," *IEEE Transactions on Power Delivery*, vol. 30, no. 3, pp. 1505–1513, 2015.

[26] M. Baù, N. Viafora, C. S. Hansen, L. M. Bergholdt Dall, T. Ebdrup, and F. Faria da Silva, "Steady state modelling of three-core wire armoured submarine cables: Power losses and ampacity estimation based on fem and iec," in *2016 51st International Universities Power Engineering Conference (UPEC)*, 2016, pp. 1–6.

[27] E. E. Zajac, "Dynamics and kinematics of the laying and recovery of submarine cable," *The Bell System Technical Journal*, vol. 36, no. 5, pp. 1129–1207, 1957.

[28] T. C. Chu, "A method to characterize the mechanical properties of undersea cables," *The Bell System Technical Journal*, vol. 62, no. 3, pp. 703–715, 1983.

[29] J. J. Valera-García and I. Atutxa-Lekue, "On the optimal design of hybrid-electric power systems for offshore vessels," *IEEE Transactions on Transportation Electrification*, vol. 5, no. 1, pp. 324–334, 2019.

Hoai Nam Le (M'19) received his M.S. and Ph.D. from the Nagaoka University of Technology, Nagaoka, Japan, in 2016 and 2019, respectively. Since 2019, he has been working as a postdoctoral researcher in Norwegian University of Science and Technology, Tronheim, Norway. He has published 20+ scientific papers in international journals and conference proceedings, and has filed two patents. The focus of his current research is on multiobjective optimization techniques for DC power distribution grid supplying power to different types of submerged loads. Dr. Le received an outstanding graduate student award in March 2019. He is a member of IEEE and IEEJ.

Elisabetta Tedeschi received the M.Sc. degree (with honors) in electrical engineering and the Ph.D. degree in industrial engineering from the University of Padova, Italy, in 2005 and 2009, respectively. From 2009 to 2011, she was a post doc researcher at the Norwegian University of Science and Technology (NTNU), working on the grid integration of offshore renewable energies. Having received a Marie Curie Fellowship, she was a Researcher at Tecnalia, Spain, from 2011 to 2013, where she worked as a principal investigator in the FP7-Sea2grid Project, related to the storage needs for the grid integration of wave energy converters. From 2013 to 2014, she was Research Scientist at SINTEF Energy and Adjunct Associate Professor at NTNU. In 2014, she became Full Professor within offshore grid at NTNU. Since 2020 she is also Full professor at the Department of Industrial Engineering of the University of Trento, Italy. She has a core competence in the design and control of energy conversion and transmission systems, with focus on offshore energy, and power-quality issues. She has led and/or contributed to more than 15 national and international scientific projects and she is the author or co-author of 2 book chapters and more than 100 journals and conference papers in the field of marine energy and energy conversion systems.